Available online at www.sciencedirect.com

SCIENCE DIRECT®

Chaos, Solitons and Fractals 30 (2006) 1250–1259

CHAOS
SOLITONS & FRACTALS

www.elsevier.com/locate/chaos

Deterministic integer multiple firing depending on initial state in Wang model

Yong Xie *, Jian-Xue Xu, Jun Jiang

Institute of Nonlinear Dynamics, MSSV, Department of Engineering Mechanics, Xi'an Jiaotong University, Xi'an 710049, PR China

Accepted 31 August 2005

Abstract

We investigate numerically dynamical behaviour of the Wang model, which describes the rhythmic activities of thalamic relay neurons. The model neuron exhibits Type I excitability from a global view, but Type II excitability from a local view. There exists a narrow range of bistability, in which a subthreshold oscillation and a suprathreshold firing behaviour coexist. A special firing pattern, integer multiple firing can be found in the certain part of the bistable range. The characteristic feature of such firing pattern is that the histogram of interspike intervals has a multipeaked structure, and the peaks are located at about integer multiples of a basic interspike interval. Since the Wang model is noise-free, the integer multiple firing is a deterministic firing pattern. The existence of bistability leads to the deterministic integer multiple firing depending on the initial state of the model neuron, i.e., the initial values of the state variables.

1. Introduction

Exploring the mechanism of neuronal information encoding is one of central problems in neuroscience. Since the shape of action potentials, i.e. spikes, is stereotyped, it hardly bears any information. Whereas only spikes have ability to propagate to the postsynaptic neuron, nowadays, it has been widely accepted that the time series of neuronal discharges, namely, the spike trains carry information about the process that generates the spikes. Moreover, the neural information is contained within the interspike interval (ISI) time series, which is the time interval between consecutive spikes [1–3]. They can highlight structure in the spike train that may not be obvious to casual observation. For experimenters, the ISI time series is easy to obtain, therefore, ISI data are often recorded in neurophysiological experiments.

There are a number of firing patterns observed in experiments. Among them, integer multiple firing (IMF) has received much attention from researchers all over the world [4–18]. An interesting feature of such firing pattern is that ISIs are roughly, but not exactly, integer multiples of a basic interspike interval. This leads to multimodal distribution of interspike intervals, and is just the reason of nomenclature of integer multiple firing. The corresponding return map exhibits a lattice structure which appears symmetric about the 45° line, an indication that there is no apparent correlation between successive ISIs [5]. There exists two distinct points of view about the mechanism underlying this kind of firing pattern: the one is stochastic resonance, the other is deterministic chaos [6–8]. According to the dynamical

* Corresponding author. Tel.: +86 29 82668751; fax: +86 29 83237910.
E-mail address: yxie@mail.xjtu.edu.cn (Y. Xie).

0960-0779/$ - see front matter © 2005 Elsevier Ltd. All rights reserved.
doi:10.1016/j.chaos.2005.08.182

mechanisms of neural excitability, neurons can be classified into two major types, i.e. Type I and Type II, although there are a huge number of biophysical mechanisms [19,20]. The IMF has been shown to occur in a neuron of Type II, which undergoes a Hopf bifurcation from the quiescent state to firing, driven by noise, with and without periodic stimulation [7–15]. Actually, a neuron of Type I, for whom the dynamical mechanism of excitability is a saddle-node bifurcation on invariant cycle, can also exhibit the IMF driven by periodic stimulation and noise [6]. The period of the stimulation is just the basic interspike interval. Here, the IMF is regarded to be induced by noise and related to stochastic resonance phenomenon. At present, it has been widely considered that stochastic resonance could play a constructive role in the neural information encoding process [4–15]. From theoretical and experimental studies, however, some neurons subjected only to periodic stimulation demonstrate the firing pattern of IMF, which is understood as a result of chaotic subthreshold dynamics [16–18].

It is very interesting that a deterministic IMF occurs in the Wang model without periodic stimulation and without noise. This point is completely different from the aforementioned IMF. In this paper, we investigate numerically the dynamical behaviour of the Wang model in detail, and, in particular, focus our attention on the IMF generated in this model.

The paper is organized as follows. In Section 2, we give the mathematical expressions of the Wang model and parameters used by us. Section 3 presents a global and local bifurcation diagrams of the Wang model as a function of the applied current I_{app} and shows numerical simulations of firing patterns at different values of I_{app}. In Section 4 shows a narrow bistable range of I_{app}, in which subthreshold and suprathreshold oscillatory states coexist. In the bistable range, there is a narrower region where the Wang model neuron exhibits the IMF; nevertheless this firing pattern of IMF depends on initial state due to bistability. At the end, some conclusions are drawn in Section 6.

2. The Wang model

The Wang model is a system of autonomous and noise-free four-dimensional ordinary differential equations, and describes the firing activities of thalamic relay neurons [21]. The equations are given by

$$
\begin{aligned}
C_m\frac{\mathrm{d}V}{\mathrm{d}t} &= -I_T - I_h - I_{Na} - I_K - I_{Na(p)} - I_L + I_{\text{app}},\\
\frac{\mathrm{d}h}{\mathrm{d}t} &= \frac{\phi_h(h_\infty(V)-h)}{\tau_h(V)},\\
\frac{\mathrm{d}H}{\mathrm{d}t} &= \frac{\phi_H(H_\infty(V)-H)}{\tau_H(V)},\\
\frac{\mathrm{d}n}{\mathrm{d}t} &= \frac{\phi_n(n_\infty(V)-n)}{\tau_n(V)},
\end{aligned}
$$

where V denotes the transmembrane voltage, h, H, n are three gating variables.

Here

$$
\begin{aligned}
&I_T = g_T S_\infty^3(V)\cdot h\cdot(V-V_{Ca})\\
&I_h = g_h\cdot H^2\cdot(V-V_h)\\
&I_{Na} = g_{Na}\cdot m_\infty^3(\sigma_{Na},V)\cdot(0.85-n)\cdot(V-V_{Na})\\
&I_K = g_K\cdot n^4\cdot(V-V_K)\\
&I_{Na(P)} = g_{Na(P)}\cdot m_\infty^3(\sigma_{Na(P)},V)\cdot(V-V_{Na})\\
&I_L = g_L\cdot(V-V_L)\\
&S_\infty(V) = 1/[1+\exp(-(V+65)/7.8)]\\
&h_\infty(V) = 1/[1+\exp((V-\theta_h)/k_h)]\\
&H_\infty(V) = 1/[1+\exp((V+69)/7.1)]\\
&n_\infty = \alpha_n/(\alpha_n+\beta_n)\\
&m_\infty = \alpha_m/(\alpha_m+\beta_m)\\
&\tau_h(V) = h_\infty(V)\exp[(V+162.3)/17.8]+20.0\\
&\tau_H(V) = 1000/[\exp((V+66.4)/9.3)+\exp(-(V+81.6)/13)]\\
&\tau_n = 1/(\alpha_n+\beta_n)\\
&\alpha_n(\sigma_K,V) = -0.01(V+45.7-\sigma_K)/\exp[-0.1(V+45.7-\sigma_K)-1]\\
&\beta_n(\sigma_K,V) = 0.125\exp[-(V+55.7-\sigma_K)/80]\\
&\alpha_m(\sigma_{Na},V) = -0.1(V+29.7-\sigma_{Na})/[\exp(-0.1(V+29.7-\sigma_{Na}))-1]\\
&\beta_m(\sigma_{Na},V) = 4\exp[-(V+54.7-\sigma_{Na})/18]
\end{aligned}
$$

The parameter values used in our calculation are

$C_m = 1,\ V_K = -80,\ V_{Ca} = 120,\ V_h = -40,\ V_L = -70,\ V_{Na} = 55,\ \phi_h = 2,\ \phi_n = 200/7,\ \phi_H = 1,\ g_h = 0.04,\ g_K = 30,$ $g_{Na} = 42,\ g_{Na(P)} = 9,\ g_L = 0.12,\ g_T = 1,\ \sigma_{Na} = 6,\ \sigma_{Na(P)} = -5,\ \sigma_K = 10,\ k_h = 5,\ \theta_h = -79.$

The applied current I_{app} is chosen as the control parameter. All conductances are in mS/cm^2 and voltages in mV; the capacity is μF/cm^2 and I_{app} in μA/cm^2. The unit of time is millisecond.

3. Bifurcation diagrams of the Wang model

Here, a continuation algorithm of predictor–corrector method is used to compute a sequence of points, which approximate the desired branches including steady solutions and limit cycles. Presently, there are many excellent software packages to calculate numerically bifurcation diagrams, such as MATCONT, AUTO and XPPAUT. We have used the XPPAUT to verify the accuracy of our computational results.

They are shown in Fig. 1. The change in membrane potential, that is, transmembrane voltage as a function of I_{app} is demonstrated. From Fig. 1(a), a global structure of bifurcation can be seen clearly, although some values of I_{app} have no significant physiological meaning. Evidently, the stable and unstable steady states approach each other, merge and disappear at $I_{app} = 2.189$ or so, where a saddle-node bifurcation occurs. Since saddle-node bifurcation is also called fold bifurcation, tangent bifurcation, limit point bifurcation, or turning point bifurcation, hereafter, therefore, we use the word ‘fold’ to indicate it in the figures for short. After this bifurcation point, the neuron exhibits periodic spiking, and this situation persists to $I_{app} = 27.180$, where a subcritical Hopf bifurcation occurs, as seen in Fig. 1(a). At $I_{app} = 62.830$ the stable and unstable limit cycles meet and annihilate one another, that is, a saddle-node bifurcation of limit cycles, which is sometimes termed fold bifurcation of limit cycles, appears. For the convenience of denotation, we still use ‘fold’ to show it in the figures. Consequently, a stable steady state coexists with a stable limit cycle from $I_{app} = 27.180$ to $I_{app} = 62.830$. In fact, the left end of the branch of the stable limit cycle terminated at $I_{app} = 2.154$, thus, there is a bistable region ranging between $I_{app} = 2.154$ and $I_{app} = 2.189$, where a stable steady state and a stable limit cycle coexist. In the rectangle of Fig. 1(a), the bifurcating behaviour is comparatively complicated. If the rectangle is magnified, it is shown in Fig. 1(b). It can be seen that the steady state loses stability via a subcritical Hopf bifurcation at $I_{app} = -1.959$. Actually, a fold bifurcation of limit cycles happens at $I_{app} = -1.962$, and a period-doubling bifurcation occurs at $I_{app} = -1.943$. These information is not seen clearly or not indicated at all in Fig. 1(b). The right Hopf bifurcation of Fig. 1(b) with $I_{app} = -0.422$ is supercritical, as seen clearly in Fig. 1(c). A subthreshold oscillation is elicited, and with increasing intensity of hyperpolarization, the amplitude of the oscillation grows. At $I_{app} = -0.472$ there is a fold bifurcation of limit cycles. In Fig. 1(b) and (c), it is evident to see that the branches of unstable limit cycles terminated at the unstable branch of the steady state. In practice, the neuron displays intricate firing patterns between the two Hopf bifurcations in Fig. 1(b) (not shown). At first, let us investigate the firing behaviour between the left Hopf bifurcation and the fold bifurcation of limit cycles in Fig. 1(b), as shown in Fig. 2. As for the firing behaviour in the region ranging from the fold bifurcation of limit cycles to the right Hopf bifurcation in Fig. 1(c), it will be stressed in the rest of the paper.

Fig. 2 shows the projection of the attractor in the h–V phase plane and time series of membrane potential corresponding to the left and right column, respectively, for different applied currents. It is clear that they are periodic bursting, which means many fast spiking riding at the crest of the slow oscillation. It is learned from Fig. 2 that the interburst interval (IBI) is prolonged with the strength of hyperpolarization increasing, that is, the bursting oscillation slows down when the degree of hyperpolarization is enhanced.

As described above, the Wang model exhibits the Type I excitability from a global view, however, it behaves Type II excitability from a local view. It is very exciting that two types of excitability concur in a neuron.

4. Bistability of membrane potential oscillation

We further consider neuronal activities of the Wang model between the fold bifurcation of limit cycles and the Hopf bifurcation, as shown in Fig. 1(c). To assure the part of I_{app} covered by these two bifurcation points to fall the region in question, allow us take a range of I_{app} from −0.5 to −0.4. Firstly, with $I_{app} = -0.5$ being the starting point, the oscillatory amplitude of the membrane potential, which implies the maximum minus minimum of the membrane potential, is calculated till $I_{app} = -0.4$ with a stepsize of 10^{-4} along the decreasing direction of hyperpolarization. Secondly, with $I_{app} = -0.4$ being the starting point, the same quantity is computed up to $I_{app} = -0.5$ with a stepsize of -10^{-4} along the increasing direction of hyperpolarization. The two computational results are superposed together, and in Fig. 3 it is clear to see that the two curves disagree with each other in the middle section from $I_{app} = -0.472$ to $I_{app} = -0.454$. In

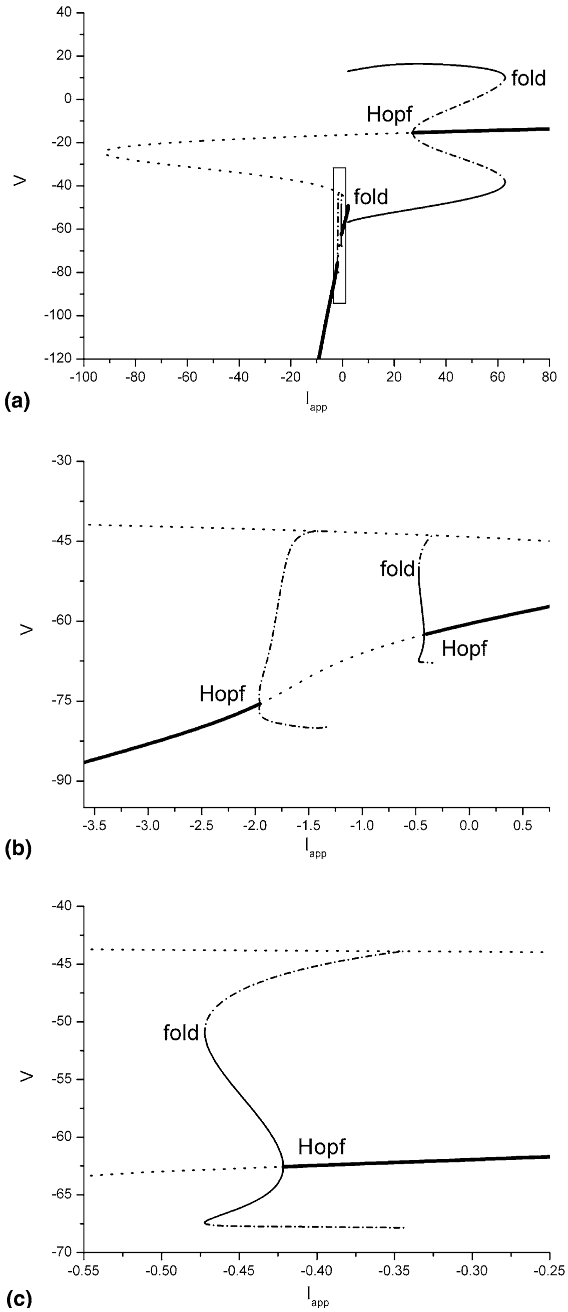

Fig. 1. Bifurcation diagram of the Wang model under the applied current I_{app}. The thick solid lines denote stable steady states, but the dotted lines indicate unstable steady states. The thin solid lines present the maxima and minima of stable limit cycles, and the short dash dotted lines are the maxima and minima of unstable limit cycles: (a) global structure of bifurcation diagram, (b) local enlargement of the rectangle in (a) and (c) magnification of the supercritical Hopf bifurcation located at the right-hand part of (b).

other words, this section is bistable. The left of the bistable range corresponds to the fold bifurcation of limit cycles, as shown in Fig. 1(c), and the right to an exterior crisis of chaotic attractor, a type of discontinuous bifurcation of a chaotic set [22–25]. Here, the exterior crisis is that a chaotic firing pattern, which will be demonstrated in the next section, disappears suddenly and becomes a subthreshold oscillation.

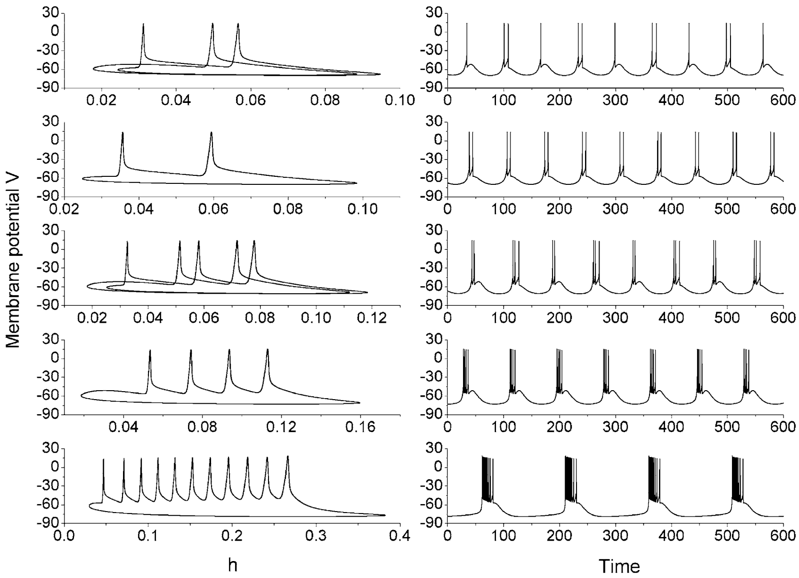

Fig. 2. The projection of the attractor in the h–V phase plane and time series of membrane potential. I_{app} corresponds to −0.6, −0.64, −0.686, −0.8, −1.2 from top to bottom.

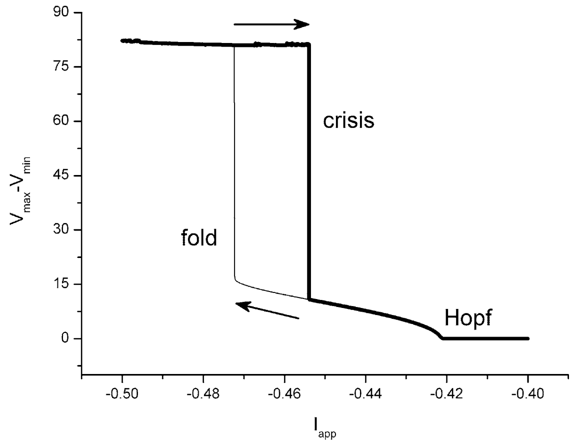

Fig. 3. The bistability range. The thin line denotes the oscillatory amplitude of membrane potential for the increasing direction of hyperpolarization, and the thick line for the decreasing direction of hyperpolarization.

The small amplitude corresponds to a subthreshold oscillation, while the large amplitude to a suprathreshold firing pattern. From Fig. 3, we can also see clearly that the subthreshold oscillation originates from the supercritical Hopf bifurcation in Fig. 1(c). For $I_{app} = -0.456$ located at the bistable range, taken $V = -62.44782$, $h = 0.03522$, $H = 0.28438$, $n = 0.11385$ as the initial state of the Wang model, the neuron exhibits a subthreshold oscillation, however, if the initial state is taken as $V = -1.65617$, $h = 0.03493$, $H = 0.11017$, $n = 0.53799$, a suprathreshold firing behaviour is observed, as seen in Fig. 4. This shows the bistability manifests itself as two distinct firing patterns obtained with the same stimulation of applied current but different initial states.

5. Integer multiple firing depending on initial state

Since the suprathreshold firing pattern is comparatively complicated in the range between the two Hopf bifurcations in Fig. 1(b), the continuation algorithm fail to compute the branch of the suprathreshold. Thus, an alternative method

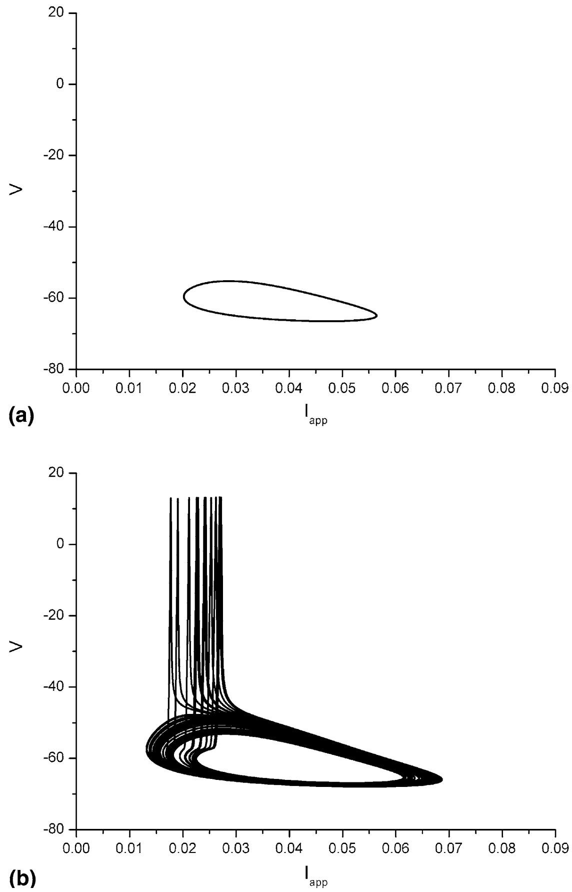

Fig. 4. Coexistence of the subthreshold oscillation and the suprathreshold firing behaviour under $I_{app} = -0.456$: (a) the initial state: $V = -62.44782$, $h = 0.03522$, $H = 0.28438$, $n = 0.11385$ and (b) the initial state: $V = -1.65617$, $h = 0.03493$, $H = 0.11017$, $n = 0.53799$.

is used to study the suprathreshold behaviour. Namely, we investigate the change in ISI as a function of I_{app} because a spike emerges for the suprathreshold case.

The change in ISI has been explored in the range from $I_{app} = -2.0$ to $I_{app} = -0.4$ along the two directions of increasing and decreasing intensity of hyperpolarization. Only in the segment of $I_{app} \in [-0.60, -0.44]$ the bifurcation of ISI is shown in Fig. 5 due to the same structure of ISI in the rest of I_{app}. It can be seen that there lies a distinct difference in the bifurcation structure of ISI versus I_{app} in a very narrow range located at the right of Fig. 5(b), which is enlarged in Fig. 5(c). Interestingly, the ISI as a function of I_{app} exhibits a multi-layer structured distribution and centers on the integer multiples of about ISI = 60 in the range of $I_{app} \in [-0.4604, -0.4540]$, which just falls in the bistable range. This shows the firing pattern with multi-layer structured distribution of the ISI depends on the initial state of the neuron.

Especially, fixed $I_{app} = -0.456$ in the range of the multi-layer structure, the membrane potential of the neuron displays an aperiodic firing when a proper initial state of the neuron is chosen, namely, it looks like random about the integer number of subthreshold cycles between each successive pair of fast spikes, as shown in Fig. 6(a). Fig. 6(b) is the corresponding series of 120 ISIs, which exhibits an irregular jump. Fig. 6(c) shows the histogram of the ISI series with a length of 50,000. This length is regarded enough long to trust the reliability of the shape of ISI histogram. It is clear that the ISI histogram is multimodal distribution with peaks at integer multiples of a basic ISI = 60, nearly equivalent to the period of the subthreshold oscillation. This is the characteristic feature of the IMF. Since the Wang model is a completely deterministic dynamical system, thus the IMF is deterministic but not stochastic. Such remarkable aperiodicity is a sign of deterministic chaos. In the h–V phase plane the phase portrait is a complicated strange attractor, as shown in Fig. 4(b), which is completely different from simple closed curves of periodic firing in the left column of Fig. 2. As a consequence, the deterministic IMF represents a chaotic firing pattern of the neuron.

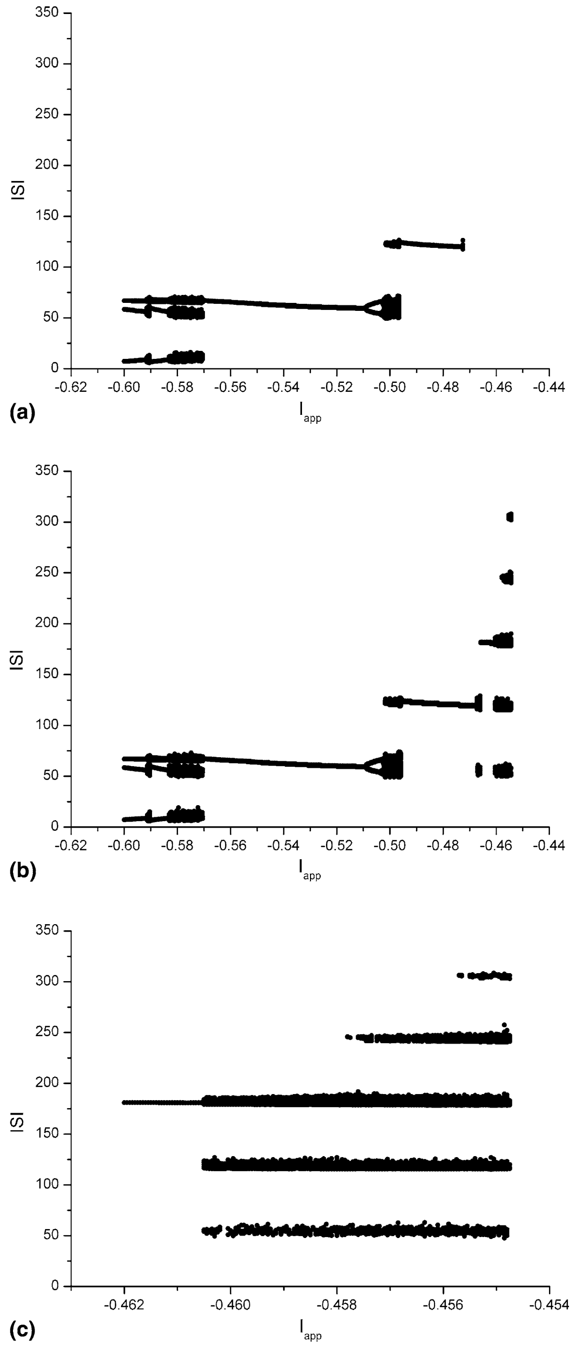

Fig. 5. Bifurcation diagram of ISI versus I_{app}: (a) the increasing direction of hyperpolarization, (b) the decreasing direction of hyperpolarization and (c) enlargement of (b) between −0.4604 and −0.4540.

Due to the existence of the bistability, whether the deterministic IMF occurs or not depends on obviously the initial state of the neuron. We freeze $H = 0.28438$ and $n = 0.11385$ to a subthreshold state, and investigate the attraction basin of the chaotic IMF in the phase plane of h–V. Here, the subthreshold values of H and n are chosen in order that the attraction basin of the subthreshold oscillation is guaranteed to exist in the phase plane of h–V. The dark area in Fig. 7 is the attraction basin of the deterministic IMF when $I_{app} = -0.456$, apparently, the white is that of the subthreshold oscillation. This shows the IMF in the Wang model is dependence of the initial state of the neuron.

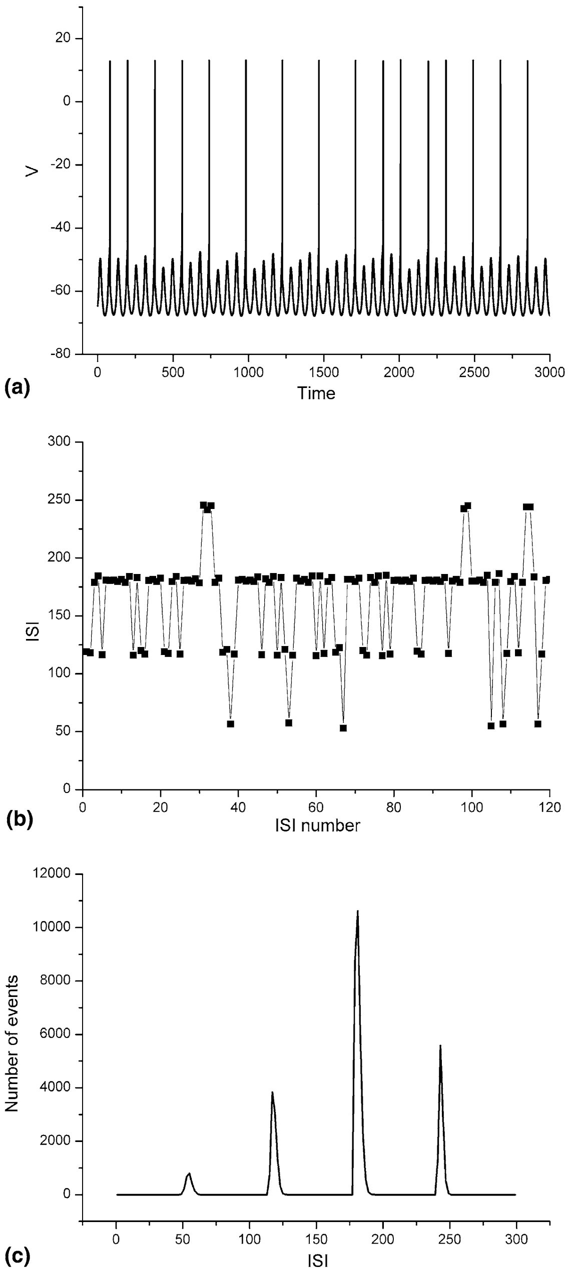

Fig. 6. Under the case of $I_{app} = -0.456$ membrane potential, aperiodic ISI series and histogram of ISI series corresponding to (a)–(c), respectively.

6. Conclusions

To sum up, the dynamical behaviour of the Wang model has been investigated in detail. We have found that the Wang possesses Type I and Type II excitability simultaneously. Namely, the neuron displays the excitability of Type I from a global view, but the excitability of Type II from a local view. A bistable range, which lies at the segment of hyperpolarization, has been uncovered, where a suprathreshold firing behaviour coexists with a subthreshold oscillation. Furthermore, there exists a narrower range just falling in the bistable range, in which the neuron exhibits a chaotic firing pattern of the IMF. We have pointed out the deterministic IMF depends on the initial state of the neuron due

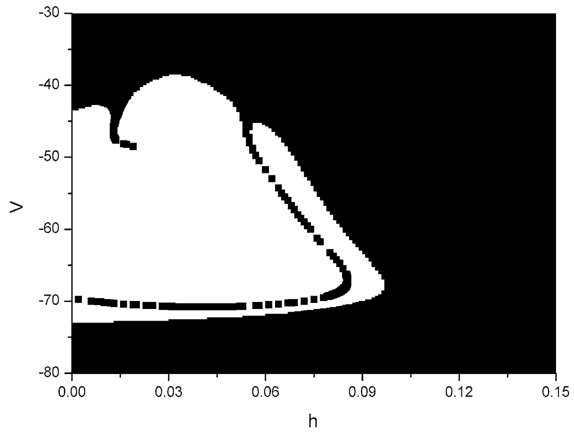

Fig. 7. Attraction basins of the IMF and the subthreshold oscillation for $I_{app} = -0.456$.

to the bistability. Consequently, the dynamical behaviour of the neuron is different along the directions of increasing and decreasing intensity of hyperpolarization. This shows it is possible that some neurons display different oscillations of the membrane potential during the application and washout processes of drugs and chemicals, or during the enhancement and weakening of the applied currents. At the same time, it is shown that the IMF can occur in an autonomous and deterministic dynamical system.

Acknowledgements

This work was supported by the National Natural Science Foundation of China (Nos. 10432010, 10472086 and 10502039).

References

[1] Rieke F, Warland D, de Ruyter van Steveninck R, Bialek W. Spikes: exploring the neural code. Cambridge: MIT Press; 1997.
[2] Reich DS, Mechler F, Purpura KP, Victor JD. Interspike intervals, receptive fields, and information encoding in primary visual cortex. J Neurosci 2000;20:1964–74.
[3] Suzuki H, Aihara K, Murakami J, Shimozawa T. Analysis of neural spike trains with interspike interval reconstruction. Biol Cybern 2000;82(4):305–11.
[4] Longtin A. Time-interval sequences in bistable systems and the noise-induced transmission of information by sensory neurons. Phys Rev Lett 1991;47(3):656–9.
[5] Longtin A. Stochastic resonance in neuron models. J Stat Phys 1993;70(1/2):309–27.
[6] Xie Y, Xu JX, Hu SJ. A novel dynamical mechanism of neural excitability for integer multiple spiking. Chaos, Solitons & Fractals 2004;21(1):177–84.
[7] Gong PL, Xu JX, Long KP, Hu SJ. Chaotic interspike intervals with multipeaked histogram in neurons. Int J Bifurcation Chaos 2002;12(2):319–28.
[8] Yang ZQ, Lu QS, Gu HG, Ren W. Integer multiple spiking in the stochastic Chay model and its dynamical generation mechanism. Phys Lett A 2002;299(5–6):499–506.
[9] Douglass JK, Wilkens L, Pantazelou E, Moss F. Noise enhancement of information transfer in crayfish mechanoreceptors by stochastic resonance. Nature 1993;265:337–40.
[10] Longtin A. Mechanisms of stochastic phase locking. Chaos 1995;5(1):209–15.
[11] Longtin A, Hinzer K. Encoding with bursting, subthreshold oscillations, and noise in mammalian cold receptors. Neural Comput 1996;8(2):215–55.
[12] Braun HA, Wissing H, Schäfer K, Hirsch MC. Oscillation and noise determine signal transduction in shark multimodal sensory cells. Nature 1994;367:270–3.
[13] Longtin A. Phase locking and resonances for stochastic excitable systems. Fluctuation Noise Lett 2002;2(3):L183–203.
[14] Yang ZQ, Lu QS. The integer multiple "fold/homoclinic" bursting induced by noise in the Chay neuronal model. Int J Nonlinear Sci Numer Simul 2005;6(1):1–6.
[15] Huber MT, Krieg JC, Dewald M, Voigt K, Braun HA. Stochastic encoding in sensory neurons: impulse patterns of mammalian cold receptors. Chaos, Solitons & Fractal 2000;11(12):1895–903.

[16] Kaplan DT, Clay JR, Manning T, Glass L, Guevara MR, Shrier A. Subthreshold dynamics in periodically stimulated squid giant axons. Phys Rev Lett 1996;76(21):4074–7.
[17] Clay JR. A novel mechanism for irregular firing of a neuron in response to periodic stimulation: irregularity in the absence of noise. J Comput Neurosci 2003;15(1):43–51.
[18] Clay JR, Shrier A. On the role of subthreshold dynamics in neuronal signaling. J Theor Biol 1999;197(2):207–16.
[19] Izhikevich EM. Neural excitability, spiking and bursting. Int J Bifurcation Chaos 2000;10(6):1171–266.
[20] Xie Y, Xu JX, Kang YM, Hu SJ, Duan YB. Critical amplitude curves for different periodic stimuli and different dynamical mechanisms of excitability. Commun Nonlinear Sci Numer Simul 2005;10(7):823–32.
[21] Wang XJ. Multiple dynamical modes of thalamic relay neurons: rhythmic bursting and intermittent phase-locking. Neuroscience 1994;59(1):21–31.
[22] Xie Y, Xu JX, Hu SJ, Kang YM, Yang HJ, Duan YB. Dynamical mechanisms for sensitive response of aperiodic firing cells to external stimulation. Chaos, Solitons & Fractals 2004;22(1):151–60.
[23] Grebogi C, Ott E, Romeiras F, Yorke JA. Critical exponents for crisis-induced intermittency. Phys Rev A 1987;36(11):5365–80.
[24] Grebogi C, Ott E, Yorke JA. Crises, sudden changes in chaotic attractors and chaotic transients. Physica D 1983;7:181–200.
[25] Grebogi C, Ott E, Yorke JA. Chaotic attractors in crisis. Phys Rev Lett 1982;48:1507–10.